Journal of Solid State Chemistry **150,** 213–220 (2000)
doi:10.1006/jssc.1999.8588, available online at http://www.idealibrary.com on IDEAL®

Solid State Cells with Buffer Electrodes for Measurement of Chemical Potentials and Gibbs Energies of Formation: System Ca–Rh–O

K. T. Jacob[1]

Department of Metallurgy and Materials Research Centre, Indian Institute of Science, Bangalore 560 012, India

and

Y. Waseda

Institute for Advanced Materials Processing, Tohoku University, Sendai 980, Japan

Received November 17, 1999; accepted November 22, 1999

The isothermal section of the phase diagram for the system Ca–Rh–O at 1273 K has been determined by equilibrating 12 compositions in the ternary and identifying phases present in quenched samples by optical microscopy, powder X-ray diffraction (XRD), and energy-dispersive analysis of X rays (EDX). One ternary compound, $CaRh_2O_4$, was found to be stable. It coexists with CaO and metallic Rh. All the alloy compositions are in equilibrium with CaO. The standard Gibbs energy of formation of $CaRh_2O_4$ and the oxygen chemical potential corresponding to the three-phase field $Rh + CaO + CaRh_2O_4$ were determined using novel designs of solid state cells incorporating yttria-stabilized zirconia as the electrolyte:

$Pt–Rh, CaO + CaRh_2O_4 + Rh/(Y_2O_3)ZrO_2/Rh + Rh_2O_3, Pt–Rh,$

$Pt–Rh, CaO + CaRh_2O_4 + Rh/(Y_2O_3)ZrO_2/O_2(0.1\ MPa), Pt–Rh.$

Buffer electrodes were introduced between reference and working electrodes to dissipate the electrochemical flux of oxygen through the solid electrolyte caused by the difference in chemical potential of oxygen at the electrodes. Polarization of the electrodes was prevented by the use of buffer electrodes. For the reaction

$$2Rh + CaO + \tfrac{3}{2}O_2 \rightarrow CaRh_2O_4,$$

$$\Delta G^\circ = \tfrac{3}{2}\Delta\mu_{O_2} = -493{,}340 + 288.67T\ (\pm 285)\ \text{J/mol}.$$

The Gibbs energy of formation of the interoxide compound from the component binary oxides is

$$\beta\text{-}Rh_2O_3 + CaO \rightarrow CaRh_2O_4,$$

$$\Delta G^\circ = -101{,}670 + 10.6T\ (\pm 290)\ \text{J/mol}.$$

Using the Neumann–Kopp rule to estimate the heat capacity of $CaRh_2O_4$, the standard enthalpy of formation and standard entropy of the compound at 298.15 K are evaluated as $-1142.3(\pm 2)$ kJ/mol and $103.2(\pm 2)$ J/mol · K, respectively.

Key Words: **phase diagram, system Ca–Rh–O; calcium rhodite, $CaRh_2O_4$; Gibbs energy, enthalpy, entropy of formation; decomposition temperature.**

1. INTRODUCTION

As a part of a larger program of research (1, 2) on M–Rh–O systems (M = alkaline earth, transition, or lanthanide element), phase relations and thermodynamic properties of condensed phases in the system Ca–Rh–O have been studied. The ternary oxides in these systems decompose before melting and have higher decomposition temperatures than the sesquioxide of rhodium. Phase equilibria in the pseudobinary system $CaO–Rh_2O_3$ have been investigated by Skrobot (3), who identified an interoxide compound, $CaRh_2O_4$. It has an orthorhombic unit cell with $a = 0.9169$, $b = 1.0745$, and $c = 0.3085$ nm, belonging to the space group $Pnam$-D_{2h}^{16} and isostructural with $CaFe_2O_4$ (4, 5). The thermodynamic properties of this compound have not been determined. Thermodynamic data on interoxide compounds are important for defining the nature of interaction of platinum group metals with refractory oxides and the conditions under which the metals can be lost in high-temperature processes.

In this study, the isothermal section of the ternary phase diagram for the system Ca–Rh–O at 1273 K has been established by identification of phases present in equilibrated samples, using optical and scanning electron microscopy,

[1] To whom correspondence should be addressed.

0022-4596/00 $35.00

powder X-ray diffraction (XRD), and energy-dispersive analysis of X rays (EDX). Using the information on phase relations, solid state emf cells were designed to measure the standard Gibbs energy of formation of $CaRh_2O_4$ from its component oxides and oxygen potential corresponding to three-phase equilibria. Special galvanic cell designs incorporating buffer electrodes were used to obtain emf values close to equilibrium.

2. EXPERIMENTAL METHODS

2.1. Materials

Fine powders of Rh and Rh_2O_3 used in this study were of 99.99% purity. The orthorhombic (β) form of Rh_2O_3 was used. The α form of Rh_2O_3, which has the corundum structure, transforms to the β form between 925 and 1125 K. Once formed, the β form does not revert to the α form. The β form of Rh_2O_3 has an orthorhombic structure, space group *Pbca* (61), with $a = 0.5148$, $b = 0.5438$, and $c = 1.4693$ nm. Calcium oxide was prepared by decomposition of 99.99% pure $CaCO_3$ at 1100 K under vacuum. Calcium metal used for preparing alloys and intermetallic compounds was 99.9% pure. Calcium rhodite ($CaRh_2O_4$) was prepared by heating pellets containing the component oxides in the appropriate ratio at 1400 K in dry oxygen for 6 days. Twice during this period, the pellets were cooled to room temperature, crushed, and repelleted for further heat treatment. The pellets were contained in an alumina crucible and supported on a sacrificial pellet of the same composition. The formation of the interoxide compound having dark violet color was confirmed by XRD. The lattice parameters of $CaRh_2O_4$ obtained in this study are $a = 0.9049$, $b = 1.0758$, and $c = 0.3095$ nm.

2.2. Determination of Phase Diagram

Phase relations were explored by equilibrating mixtures of different elements or compounds at 1273 K, followed by quenching in liquid nitrogen or chilled mercury and phase identification. Thus, 12 compositions were equilibrated for periods up to 5 days. The samples were quenched, ground to -325 mesh, and repelleted twice during this period. The phase compositions of the samples were found to be unaltered by further heat treatment. The overall compositions of the samples are shown on the Gibbs triangle of Fig. 1.

Two arrangements were used for equilibrating samples at high temperature. Several mixtures containing CaO, Rh_2O_3, and $CaRh_2O_4$ were equilibrated in pure oxygen at 0.1 MPa, using an apparatus described earlier (6). The samples were held in recrystallized alumina crucibles lined with Rh_2O_3. The sample pellets were kept on sacrificial disks of the same composition. The mass of each pellet was determined before and after equilibrium. Mixtures containing metals or alloys were equilibrated in closed iron crucibles

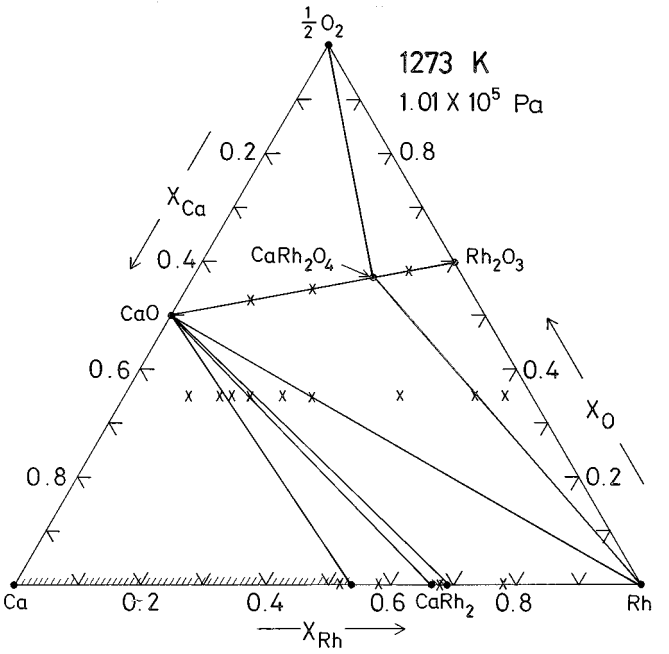

FIG. 1. Isothermal section of the phase diagram for the system Ca–Rh–O at 1273 K. The average composition of the samples used in this study is represented by *X*.

under flowing inert gas. The mixtures were prepared in an inert atmosphere glove box. The oxygen partial pressure in the inert gas was less than 10^{-10} Pa. The pellets made from each mixture were contained in a thoria crucible placed inside the larger closed iron crucible. Each set of pellets was placed on a sacrificial disk of the same composition to avoid possible contamination by the thoria crucible. In many cases, samples of the same overall composition were made, using different starting materials. Phases present in quenched samples were identified by optical and scanning electron microscopy, EDX, and XRD.

2.3. Measurement of Gibbs Energy of Formation of $CaRh_2O_4$

The reversible emf of the solid state cell,

$$\text{Pt–Rh, CaO} + \text{CaRh}_2\text{O}_4 + \text{Rh}/(\text{Y}_2\text{O}_3)\text{ZrO}_2/\text{Rh} + \text{Rh}_2\text{O}_3\text{, Pt–Rh,} \qquad \text{[I]}$$

was measured as a function of temperature in the range 890 to 1310 K. The cell is written such that the right-hand electrode is positive. Because of the difference in the chemical potential of oxygen between the reference on the right side and working electrode on the left side of the cell, there is always a small flux of oxygen through the zirconia electrolyte separating them, even in the absence of physical

porosity. The small electrochemical permeability is caused by trace electronic conductivity ($t_e < 0.01$) in the solid electrolyte. It occurs by the coupled transport of oxygen ions and electrons (or holes) in the solid electrolyte under the oxygen potential gradient. The very small but finite electronic conductivity acts as a internal short circuit.

The electrochemical flux of oxygen can cause polarization of multiphase solid electrodes. The chemical potential of oxygen in the microsystem at the electrolyte/electrode interface can be altered by the flux through the electrolyte. Buffer electrodes can be designed to act as a sink for this flux and prevent it from reaching the measuring electrodes.

A new four-compartment design of the cell was used to enhance the accuracy of measurement. A schematic diagram of the cell is shown in Fig. 2. It consisted of four distinct compartments, separated by yttria-stabilized zirconia tubes and crucibles. The cell can be represented as

Pt–Rh $O_2(P'_{O_2})$ measuring electrode	$(Y_2O_3)ZrO_2$ no O^{2-} flux	$O_2(P''_{O_2})$ $P''_{O_2} \approx P'_{O_2}$ measuring buffer electrode	$(Y_2O_3)ZrO_2$ $\leftarrow$ O^{2-} flux	$O_2(P'''_{O_2})$ $P'''_{O_2} \approx P''''_{O_2}$ reference buffer electrode	$(Y_2O_3)ZrO_2$ no O^{2-} flux	Pt–Rh $O_2(P''''_{O_2})$ reference electrode.

The buffer electrode adjacent to the reference electrode initially has the same composition and chemical potential as the reference electrode. Without a driving force, there is no transport of oxygen between these compartments, and the reference electrode is immune to polarization. Similarly, the buffer electrode adjacent to the measuring electrode initially has the same chemical potential as the measuring electrode. The oxygen potential gradient exists only across the zirconia tube separating the two buffer electrodes. Polarization effects are therefore confined to the buffer electrodes. The oxygen chemical potential gradient causes coupled flow of oxygen ions and trace electronic carriers (holes and electrons) through the solid electrolyte. Although a solid electrolyte is a predominantly ionic conductor, with oxygen ion transport number greater than 0.99, there is present always a small but finite concentration of holes and electrons. The concentration of these electronic defects is a function of temperature and oxygen partial pressure. The electrochemical flux of oxygen through the electrolyte is limited by the concentration of electronic defects. During the course of the experiment, the oxygen chemical potential of the buffer electrodes may thus change slightly from its initial value. The emf, which is related to the oxygen chemical potential difference between the measuring and reference electrodes, is unaffected. A single buffer electrode between measuring and reference electrodes was suggested recently by Lundberg and Rosen (7). However, unless one of the electrodes is nonpolarizable, their design does not completely solve the polarization problem caused by electrochemical transport of oxygen through the oxide solid electrolyte.

The reference electrode was prepared by compacting an intimate mixture of fine powders of Rh and Rh_2O_3 in the molar ratio 1 : 1.5 against the closed end of a yttria-stabilized zirconia tube, with a Pt–30%Rh lead embedded in the mixture. The reference buffer electrode was prepared in an identical fashion, using a stabilized zirconia tube of larger diameter. The smaller zirconia tube containing the reference electrode was placed inside the larger tube. Alumina sheaths were used to insulate the Pt–30%Rh leads. The top of the larger zirconia tube was closed with a tight-fitting bell-shaped Pyrex tube, which supported two W electrode connections sealed into glass. The joint between the bell and the zirconia tube was sealed with De Khotinsky cement. A spring placed between the bell and the inner zirconia tube applied pressure on the buffer electrode. The assembled half-cell containing the reference electrode and its buffer was first evacuated using a side-arm tube shown in the diagram, heated to ~ 400 K, and then flame-sealed under vacuum.

The measuring electrode was prepared by compacting a mixture of CaO, $CaRh_2O_4$, and Rh in the molar ratio 1 : 1.5 : 1 in a stabilized zirconia crucible, with a Pt–30%Rh lead buried in it. The measuring-buffer electrode was prepared in the same way inside a crucible with smaller diameter. The smaller zirconia crucible containing the buffer electrode was placed over the measuring electrode, and the space between was filled with the three-phase electrode mixture. The measuring half-cell with the buffer was assembled inside a vertical quartz enclosure.

The reference half-cell assembly contained in the larger zirconia tube was placed over the measuring-buffer electrode and pressed down by means of a second metal spring between the bell and the top Pyrex cover. The top cover supported four W-glass seals through which electrical connections to the four electrodes were made. All electrode connections were silver-soldered. Finally, the top cover was cemented in place by melting the De Khotinsky cement in the ring container shown in the diagram. The cement

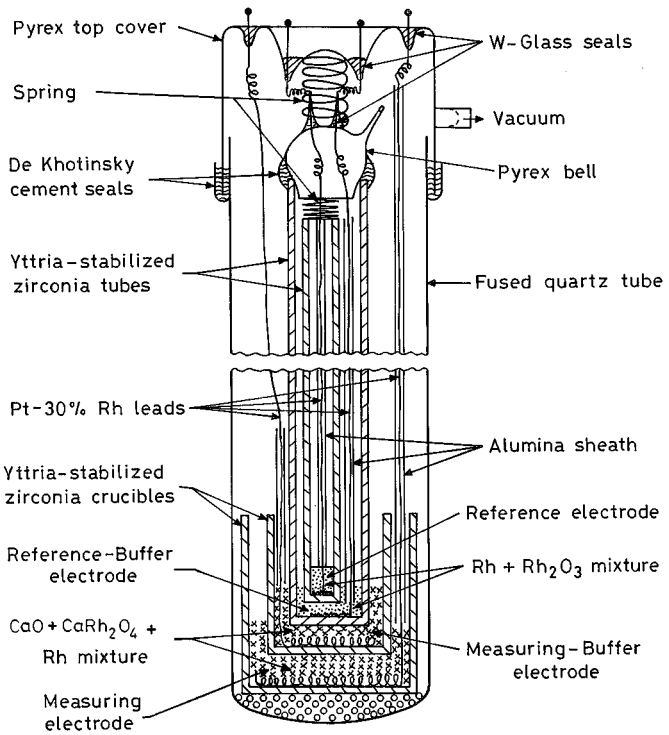

FIG. 2. Schematic diagram of the new apparatus used for measuring free energy of formation of $CaRh_2O_4$ at high temperatures. The cell has two buffer electrodes in addition to measuring and reference electrodes.

was allowed to solidify while pressing the top cover against the spring. Then the outer quartz enclosure was also evacuated from a side-arm tube and flame-sealed under vacuum.

Except for the addition of two buffer electrode compartments, the general features of the apparatus were similar to those of the apparatus used by Charette and Flengas (8). Since the oxygen partial pressure over the electrodes used in this study become appreciable at high temperatures, the use of a closed system was found to be more suitable than designs that employ either dynamic vacuum or inert gas flow. Yttria-stabilized zirconia was selected as the solid electrolyte, since it does not undergo "aging" in the temperature range covered in this study. The cubic solid solution phase of calcia- or magnesia-stabilized zirconia undergoes gradual phase transformation at the temperatures employed in this study, with consequent deterioration of its electrochemical properties.

The entire assembly shown in Fig. 2 was placed inside a vertical resistance furnace, with the electrodes located in the even-temperature zone (± 1 K). The upper part of the assembly, where cement seals were located, was at room temperature during measurements. A Faraday cage, made from stainless-steel foil, was placed between the furnace and the cell assembly. The foil was grounded to minimize induced emf on cell leads. The temperature of the furnace was controlled to ± 1 K. The temperature was measured with a Pt/Pt–13%Rh thermocouple, calibrated against the melting point of gold. The cell potentials were measured with a high-impedance digital voltmeter with a sensitivity of ± 0.01 mV. The potential readings were corrected for small thermal emfs, measured separately using a symmetric cell configuration with identical electrodes.

2.4. Measurement of Chemical Potential of Oxygen

The oxygen chemical potential corresponding to the equilibrium between three condensed phases Rh, $CaRh_2O_4$, and CaO was measured using a solid state cell with three electrodes. Pure oxygen gas at a pressure of 0.1 MPa was used as the reference electrode, since it is the primary oxgen potential standard. The oxygen gas flowing at 2 ml/s over RuO_2/Pt electrode forms a nonpolarizable system. Therefore, there is no need for a reference buffer electrode. The cell design can be represented as

Pt–Rh, $O_2(P'_{O_2})$ measuring electrode	$(Y_2O_3)ZrO_2$ no O^{2-} flux	$O_2(P''_{O_2})$, buffer electrode $P''_{O_2} \approx P'_{O_2}$	$(Y_2O_3)ZrO_2$ $\leftarrow$ O^{2-} flux	$O_2(P'''_{O_2})$, Pt–Rh reference electrode

A schematic diagram of the apparatus used for measurements is shown in Fig. 3. Details of the cell assembly are similar to those described in the previous section. Two stabilized-zirconia tubes were used: one housing the oxygen reference electrode and the other containing the three-phase measuring electrode. The measuring-buffer electrode was contained in the stabilized-zirconia crucible. The reversible emf of the cell,

$$\text{Pt–Rh, } CaO + CaRh_2O_4 + Rh/(Y_2O_3)ZrO_2/O_2 \text{ (0.1 MPa), Pt–Rh,} \quad \text{[II]}$$

was measured as a function of temperature.

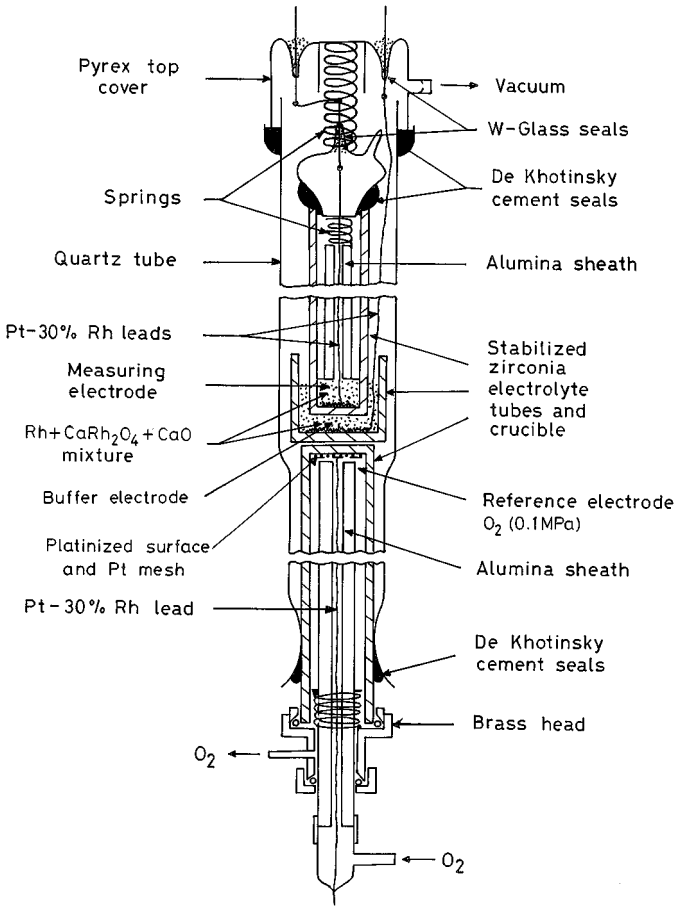

FIG. 3. Schematic diagram of the three-electrode cell assembly for measuring oxygen potential relative to pure oxygen gas at 0.1 MPa as the reference.

3. RESULTS AND DISCUSSION

3.1. Phase Diagram

The isothermal section of the phase diagram for the system Ca–Rh–O at 1273 K, composed from the results of this study, is shown in Fig. 1. There is only one stable oxide, Rh_2O_3, along the Rh–O binary. Thermodynamic data given in the compilation of Kancke *et al.* (9) indicate that the vapor pressure of RhO in the system is negligible. For example, the vapor pressure of RhO over the phase mixture Rh + Rh_2O_3 at 1300 K is 7.4×10^{-8} Pa. Along the Ca–O binary, there is only one stable oxide, CaO. One intermetallic phase $CaRh_2$ with variable composition was identified along with the Ca–Rh binary. At 1273 K, the composition of this phase varies from 66.7 to 69.3 at.% Rh. The liquid alloy phase extends upto 54 at.% Rh. A complete phase diagram for the binary system Ca–Rh is not available (10). There is one ternary oxide, $CaRh_2O_4$, along the pseudobinary CaO–Rh_2O_3. The XRD patterns of $CaRh_2O_4$ in different phase fields are almost identical. The ratio Rh/(Mg + Rh) in $CaRh_2O_4$ determined by EDX is 0.67 ($\pm$ 0.01) in the various phase fields. There is no significant solid solubility between the oxide phases. The oxygen content of the ternary oxide determined from the mass loss on reduction by hydrogen to a mixture of CaO and Rh agrees exactly with the formula $CaRh_2O_4$. There are two three-phase fields involving the ternary oxide and rhodium metal: $CaRh_2O_4$ + CaO + Rh and $CaRh_2O_4$ + Rh_2O_3 + Rh. All the alloys are in equilibrium with pure CaO.

3.2. Thermodynamic Properties of $CaRh_2O_4$

The reversibility of the emf of cell I was established by microcoulometric titration in both directions. A small current ($\sim$50 μA) was passed through the cell, using an external potential source for $\sim$5 min. The open-circuit emf was subsequently monitored as a function of time. The emf was found to return to the steady value before each titration. During the titration, the chemical potential of oxygen at each electrode was displaced from equilibrium by an essentially infinitesimal amount. Since the electrodes returned to the same potential after displacement from equilibrium in opposite directions, reversibility of the cell was confirmed. The emf measured between the two buffer electrodes was always lower by 2 to 3 mV than that between the measuring and reference electrodes. The emf between the two buffer electrodes is identical to that of a conventional two-compartment cell. When microcoulometric titration was done between the buffer electrodes, there was a small hysteresis effect of $\sim$2 mV. This indicates a finite polarization effect due to the flux of oxygen from the reference-buffer to the measuring-buffer electrodes. Although both electrode systems are invariant at constant temperature, measurement of their oxygen potential using the conventional solid-state cell can result in a small but significant systematic error. The flux of oxygen through the electrolyte disturbs slightly the oxygen potential in the microsystem at the electrolyte/electrode interface. The use of the four-compartment design improves the accuracy by insulating the measuring and reference electrodes from polarization effects.

The reversible emf of cell I is shown in Fig. 4 as a function of temperature. The different symbols represent results from separate experiments. Emf was reproducible on temperature cycling. The emf is seen to decrease slightly with temperature. The least-squares regression analysis of the emf yields the expression

$$E_{\mathrm{I}} = 175.6 - 1.83 \times 10^{-2} T \ (\pm 0.5)\ \mathrm{mV}. \qquad [1]$$

The uncertainty limit is based on twice the standard error estimate and error in temperature measurement. The oxygen chemical potential at the right-hand electrode of cell I is determined by the reaction

$$\beta\text{-}Rh_2O_3 \rightleftarrows 2\ Rh + \tfrac{3}{2}O_2. \qquad [2]$$

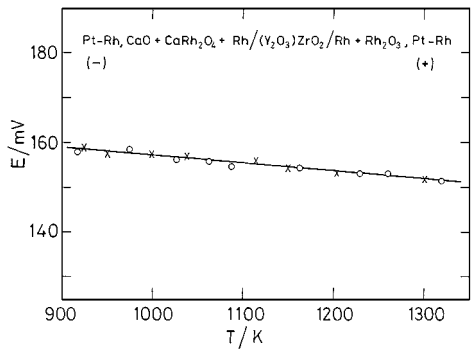

FIG. 4. Temperature dependence of emf of cell I.

At the left-hand electrode, the oxygen potential is fixed by the equilibrium between the three condensed phases

$$2\ \mathrm{Rh} + \mathrm{CaO} + \tfrac{3}{2}\mathrm{O_2} \rightleftarrows \mathrm{CaRh_2O_4}. \qquad [3]$$

The overall cell reaction is

$$\mathrm{CaO} + \beta\text{-}\mathrm{Rh_2O_3} \rightarrow \mathrm{CaRh_2O_4}. \qquad [4]$$

The standard Gibbs free energy change for this reaction is obtained directly from the emf:

$$\Delta G_4^\circ = -nFE_{\mathrm{I}} = -101{,}670 + 10.6T\ (\pm 300)\ \mathrm{J/mol}, \qquad [5]$$

where $n = 6$ is the number of electrons involved in the electrode reactions, and F is the Faraday constant. The temperature-independent term in Eq. [5] gives the enthalpy change for reaction [4] at a mean temperature of 1100 K. The enthalpy of formation of $CaRh_2O_4$ from its component oxides CaO and β-Rh_2O_3 is $-101.7\ (\pm 1)$ kJ mol^{-1}. The entropy of formation of $CaRh_2O_4$ from its component oxides is $-10.6\ (\pm 1)$ J K^{-1} mol^{-1} at 1100 K. There are no data in the literature with which these values can be compared. It would be useful to confirm the results obtained in this study by calorimetric techniques. The enthalpy of formation can be measured by combustion or solution calorimetry. The entropy of $CaRh_2O_4$ can be obtained from the measurement of heat capacity as a function of temperature. A solid state galvanic cell based on CaF_2 as the electrolyte provides an alternative method for measuring the free energy of formation of $CaRh_2O_4$ at high temperatures.

3.3. Oxygen Potential Corresponding to Three-Phase Equilibrium

The reversible emf of cell II is plotted as a function of temperature in Fig. 5. Emfs obtained in each experiment are denoted by a characteristic symbol. Within experimental uncertainty, the emf is a linear function of temperature. The least-squares regression analysis gives

$$E_{\mathrm{II}} = 852.1 - 0.4986T\ (\pm 0.5)\ \mathrm{mV}. \qquad [6]$$

The oxygen chemical potential corresponding to the three-phase equilibrium between Rh, CaO, and $CaRh_2O_4$ can be obtained directly from the emf of cell II:

$$\Delta\mu_{\mathrm{O_2}} = -4FE_{\mathrm{II}} = -328{,}890 + 192.45T\ (\pm 190)\ \mathrm{J/mol}. \qquad [7]$$

The oxygen potential is defined by the reaction

$$\tfrac{4}{3}\mathrm{Rh} + \tfrac{2}{3}\mathrm{CaO} + \mathrm{O_2} \rightleftarrows \tfrac{2}{3}\mathrm{CaRh_2O_4}, \qquad [8]$$

for which $\Delta G_8^\circ = \Delta\mu_{\mathrm{O_2}}$, when Rh, CaO, and $CaRh_2O_4$ are at unit activity. Combining Eqs. [4] and [8], the standard free energy of orthorhombic Rh_2O_3 can be derived as

$$\Delta G_{\mathrm{f}}^\circ\ (\mathrm{Rh_2O_3},\ \beta) = -391{,}670 + 278.07T\ (\pm 410)\ \mathrm{J/mol}. \qquad [9]$$

In the temperature range 900 to 1300 K, the Gibbs energy of formation of Rh_2O_3 has been measured directly using an experimental arrangement similar to that for cell II (1). The results of the direct measurement can be represented by the equation

$$\Delta G_{\mathrm{f}}^\circ\ (\mathrm{Rh_2O_3},\ \beta) = -396{,}365 + 282.0T\ (\pm 200)\ \mathrm{J/mol}. \qquad [10]$$

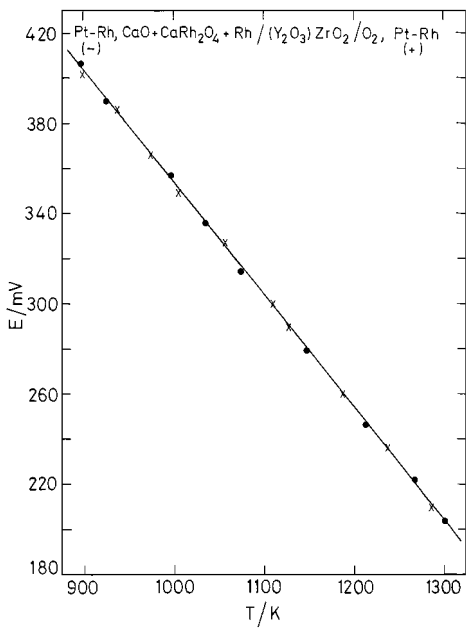

FIG. 5. Variation of reversible emf of cell II with temperature.

Although the "second law" enthalpy and entropy of formation of β-Rh_2O_3 derived from the two sets of data are slightly different, the Gibbs energies of formation at high temperature (900–1300 K) are in good agreement ($\pm$1 kJ/mol). This close correspondence provides an internal check of the accuracy of emf measurements. The Gibbs energies of formation obtained in this study are also in excellent agreement with recent measurements of Nell and O'Neill (11). The data for Rh_2O_3 given in current thermodynamic compilations (9, 12), based on older measurements, are incorrect (13). The recent reassessment of data for β-Rh_2O_3 suggests a revision of standard enthalpy of formation at 298.15 K from -355.64 to -405.53 kJ/mol. The standard entropy of β-Rh_2O_3 at 298.15 K is revised from 106.27 J/mol·K given in the compilations (9, 12) to 75.69 J/mol·K (13). The standard enthalpy of formation and standard entropy of $CuRh_2O_4$ at 298.15 K can be computed from the results of this study at high temperatures by using the Neumann–Kopp rule to estimate its heat capacity. For this purpose, the enthalpy of formation and entropy of CaO is taken from Barin (12); corresponding information for Rh_2O_3 is from Ref. (13). The standard enthalpy of formation of $CaRh_2O_4$ from elements at 298.15 K computed from Eq. [5] is -1142.3 ($\pm$2) kJ/mol. The corresponding standard entropy of $CaRh_2O_4$ at 298.15 K is 103.2 ($\pm$2) J/mol·K.

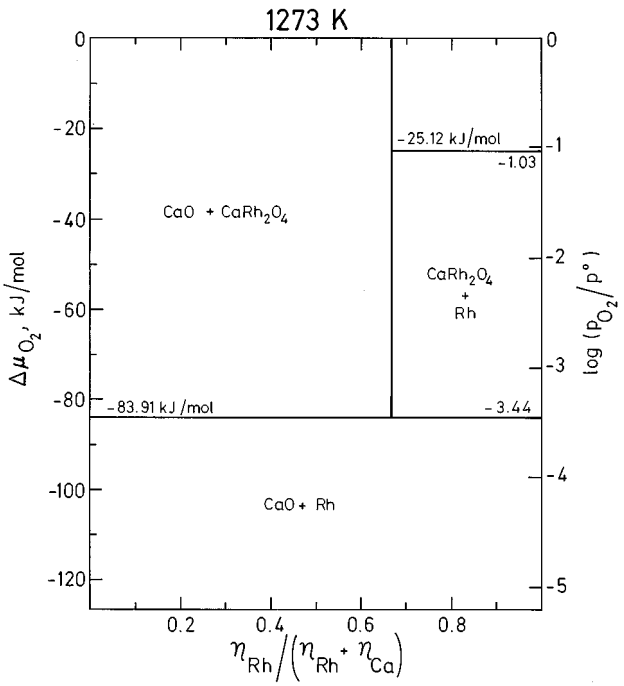

FIG. 6. Oxygen chemical potential diagram for the system Ca–Rh–O at 1273 K.

3.4. *Decomposition Temperature*

The phase diagram indicates that the compound $CaRh_2O_4$ would decompose according to reaction [3], when the oxygen partial pressure is lowered below the equilibrium value. The oxygen potential corresponding to this decomposition has been measured as a function of temperature. Equation [7] suggests a decomposition temperature of 1709 ($\pm$3) K for $CaRh_2O_4$ in pure oxygen at standard pressure of 0.1 MPa. The decomposition in air under equilibrium conditions would occur at 1601 ($\pm$3) K. The calculated decomposition temperature is 8 K higher than that suggested by Skrobot (3), who reports an uncertainty of $\pm$5 K in their temperature measurement.

3.5. *Computation of Phase Diagrams*

An oxygen potential diagram for the system Ca–Rh–O at 1273 K, composed from the results obtained in this study, is shown in Fig. 6. The composition of phases is represented by the cationic fraction $\eta_{Rh}/(\eta_{Rh}+\eta_{Ca})$, where η_i represents moles of component *i*. Since oxygen is not included in the composition parameter, information on oxygen nonstoichiometry cannot be displayed on the diagram. Nevertheless, the diagram provides useful information on the oxygen potential range for the stability of various phases. The diagram is complementary to the Gibbs triangle representation of phase relations in a ternary system, where phase compositions can be clearly displayed. All the topological rules of construction for conventional temperature–composition phase diagrams are applicable to the oxygen potential diagram shown in Fig. 6.

When three condensed phases and a gas phase coexist at equilibrium in a ternary system such as Ca–Rh–O, the system is monovariant; at a fixed temperature, three condensed phases coexist only at a unique partial pressure of oxygen. The three-phase equilibria are therefore represented by horizontal lines on the diagram. The equilibria at very low oxygen potentials between alloys and CaO are not shown in Fig. 6 since thermodynamic data for intermetallics required for the calculation are not available. These low oxygen potentials cannot be measured easily since they are well below the ionic conduction domain of oxide solid electrolytes. Similar diagrams at other temperatures can be readily computed from the thermodynamic data.

Phase relations can also be obtained as a function of temperature at constant oxygen partial pressure. The computed phase diagrams in air ($P_{O_2} = 2.12 \times 10^4$ Pa) and at an oxygen partial pressure of 0.101 Pa are shown in Fig. 7. It is clear that the temperature–composition phase diagram is very sensitive to oxygen partial pressure in the ambient atmosphere. The decomposition temperature of $CaRh_2O_4$ is considerably higher than that of Rh_2O_3 at all partial pressures of oxygen.

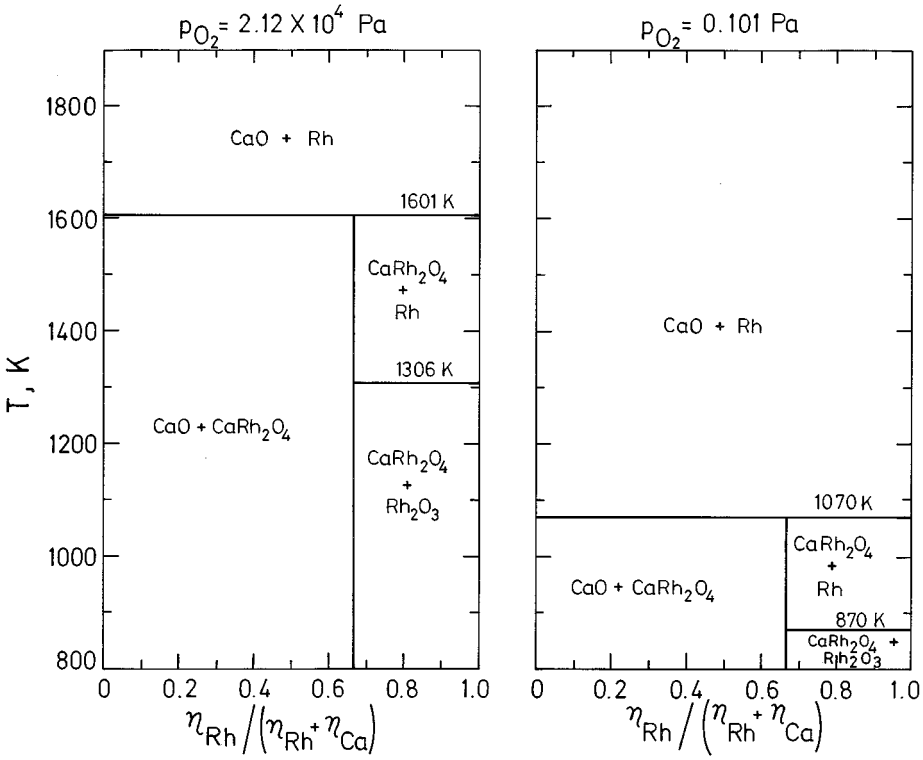

FIG. 7. Temperature–composition phase diagram for the system Ca–Rh–O at two different oxygen partial pressures ($P_{O_2} = 2.12 \times 10^4$ and 0.101 Pa).

4. SUMMARY

A study of phase relations in the system Ca–Rh–O indicates that only one ternary compound, $CaRh_2O_4$, is present at 1273 K. A nonstoichiometric intermetallic compound $CaRh_2$ is present along the Ca–Rh binary. The standard Gibbs energy of formation of $CaRh_2O_4$ from component oxides has been measured as a function of temperature:

$$\Delta G^{\circ}_{f,ox}\,(CaRh_2O_4) = -101{,}670 + 10.6T\ (\pm 290)\ \text{J/mol}.$$

The orthorhombic form of Rh_2O_3 is the reference state for the sesquioxide. A special design of the solid state cell, incorporating four electrode compartments, has been developed to avoid systematic error caused by polarization of the electrodes. The oxygen potential corresponding to the decomposition of $CaRh_2O_4$ to Rh, CaO, and O_2 has been obtained as a function of temperature:

$$\Delta\mu_{O_2} = -328{,}890 + 192.45T\ (\pm 190)\ \text{J/mol}.$$

The standard enthalpy of formation and standard entropy of $CaRh_2O_4$ at 298.15 K are evaluated from the high-temperature data. Using thermodynamic information on the stability of phases, phase relations in the system Ca–Rh–O have been computed as a function of oxygen potential and temperature.

REFERENCES

1. K. T. Jacob and M. V. Sriram, *Metall. Mater. Trans. A* **25,** 1347 (1994).
2. K. T. Jacob and Y. Waseda, *J. Am. Ceram. Soc.* **78,** 440 (1995).
3. V. N. Skrobot, *Russ. J. Inorg. Chem.* **24,** 1209 (1989).
4. I. S. Shaplygin, I. I. Prosychev, V. B. Lazarev, *Russ. J. Inorg. Chem.* **31,** 1649 (1986).
5. J. Preudhomme, *C.R. Seances Acad. Sci. C* **271,** 1073 (1970).
6. K.T. Jacob and T. Mathews, *J. Mater. Chem.* **1,** 545 (1991).
7. M. Lundberg and E. Rosen, *J. Am. Ceram. Soc.* **75,** 1452 (1992).
8. G. G. Charette and S. N. Flengas, *J. Electrochem. Soc.* **115,** 796 (1969).
9. O. Knacke, O. Kubaschewski, and K. Hesselmann, "Thermodynamic Properties of Inorganic Substances," 2nd ed., Vols. I and II. Springer-Verlag, Berlin, 1991.
10. T. B. Massalski, P. R. Subramanian, H. Okamoto, and L. Kacprzak, "Binary Alloy Phase Diagrams," 2nd ed., Vols. 1 and 2. ASM International, Materials Park, OH,1990.
11. J. Nell and H. St. C. O'Neill, *Geochim. Cosmochim. Acta* **61,** 4159 (1997).
12. I. Barin, "Thermochemical Data for Pure Substances," Parts I and II. VCH, Weinheim/New York, 1989.
13. K. T. Jacob, T. Uda, T. H. Okabe, and Y. Waseda, *High Temp. Mater. Process.*, 1999 (in press).